Journal of Organic and Pharmaceutical Chemistry

Original Research

OPEN ACCESS
Freely available online on
http://ophcj.nuph.edu.ua

UDC 547.775+547.722+577.152.1

A. V. Beiko, O. L. Kobzar, M. V. Kachaeva, S. G. Pilyo, V. Yu. Tanchuk, A. I. Vovk

V. P. Kukhar Institute of Bioorganic Chemistry and Petrochemistry of the National Academy of Sciences of Ukraine, 1 Academician Kukhar str., 02094 Kyiv, Ukraine

Inhibition of Xanthine Oxidase by Pyrazolone Derivatives Bearing a 4-(Furan-2-yl)benzoic Acid Moiety

Abstract

The pyrazolone-based 4-(furan-2-yl)benzoic acids have been synthesized and studied as xanthine oxidase inhibitors. This enzyme is one of the therapeutic targets for the treatment of hyperuricemia and related diseases. The compounds studied have found to exhibit low micromolar IC_{50} values relative to the enzyme *in vitro*, depending on substituents in position 3 of the pyrazolone ring. However, the inhibitory effects observed are reduced in the presence of bovine serum albumin or Tween-80. Among the pyrazolone derivatives synthesized, 4-(5-((3-methyl-5-oxo-1-phenyl-1,5-dihydro-4*H*-pyrazol-4-ylidene)methyl)furan-2-yl)benzoic acid has been found to be the most potent inhibitor of xanthine oxidase. Kinetic results have shown that this compound is a mixed-type inhibitor with higher affinity to the free enzyme than to the enzyme-substrate complex. The results of the molecular docking and molecular dynamics show that the carboxylic group of the inhibitor can form a salt bridge with Arg880 and a hydrogen bond with Thr1010. These interactions can be key factors in the enzyme-inhibitor complex stabilization.

Keywords: xanthine oxidase; inhibition; pyrazolone; benzoic acid; molecular docking; molecular dynamics

А. В. Бейко, О. Л. Кобзар, М. В. Качаєва, С. Г. Пільо, В. Ю. Танчук, А. І. Вовк

Інститут біоорганічної хімії та нафтохімії ім. В. П. Кухаря Національної академії наук України, вул. Академіка Кухаря, 1, Київ, 02094, Україна

Інгібування ксантиноксидази похідними піразолону, що містять фрагмент 4-(фуран-2-іл)бензойної кислоти

Анотація

4-(Фуран-2-іл)бензойні кислоти з фрагментом піразолону було синтезовано та досліджено як інгібітори ксантиноксидази. Цей ензим є однією з терапевтичних мішеней для лікування гіперурикемії та супутніх захворювань. Вивчені сполуки демонстрували низькомікромолярні значення IC_{50} щодо ензиму *in vitro*, залежно від замісників у положенні 3 піразолонового кільця. Однак спостережувані інгібувальні ефекти знижувались за наявності бичачого сироваткового альбуміну або твіну-80. Серед синтезованих похідних піразолону 4-(5-((3-метил-5-оксо-1-феніл-1,5-дигідро-4*H*-піразол-4-іліден)метил)фуран-2-іл)бензойна кислота виявилась найпотужнішим інгібітором ксантиноксидази. Кінетичні дослідження засвідчили, що ця сполука є інгібітором змішаного типу з більшою спорідненістю до вільного ензиму, ніж до ензим-субстратного комплексу. Результати молекулярного докінгу і молекулярної динаміки свідчать про те, що карбоксильна група інгібітора може формувати сольовий місток із залишком Arg880 і водневий зв'язок із залишком Thr1010. Ці взаємодії можуть бути ключовими факторами стабілізації комплексу ензим-інгібітор.

Ключові слова: ксантиноксидаза; інгібування; піразолони; бензойна кислота; молекулярний докінг; молекулярна динаміка

Citation: Beiko, A. V.; Kobzar, O. L.; Kachaeva, M. V.; Pilyo, S. G.; Tanchuk, V. Yu.; Vovk, A. I. Inhibition of xanthine oxidase by pyrazolone derivatives bearing a 4-(furan-2-yl)benzoic acid moiety. *Journal of Organic and Pharmaceutical Chemistry* **2023**, *21* (4), 27–35.
https://doi.org/10.24959/ophcj.23.298726
Received: *1 October 2023*; **Revised:** *23 October 2023*; **Accepted:** *28 October 2023*

Funding: The work was founded by the National Academy of Sciences of Ukraine.
Conflict of interests: The authors have no conflict of interests to declare.

■ Introduction

Xanthine oxidase (XO) is the main cytosolic molybdenum-containing enzyme of the purine catabolism that catalyzes the transformation of hypoxanthine to xanthine and uric acid. Increased xanthine oxidase activity is not only the cause of hyperuricemia and gout, but also the cause of hyperuricemia-related disorders, such as metabolic syndrome, renal and cardiovascular diseases, diabetes, hypertension, and cancer. In addition, the enzymatic reaction is accompanied by the formation of reactive oxygen species causing oxidative stress and systemic inflammation [1]. Currently, FDA-approved drugs, such as allopurinol and febuxostat (as well as topiroxostat approved in Japan), are widely used in the treatment of the diseases associated with the enhanced XO activity. However, these drugs possess significant adverse effects and are not suitable for a long-term treatment of asymptomatic hyperuricemia. Thus, the development of new XO inhibitors is needed [2]. For this reason, the derivatives of imidazole, pyrazole, thiazole, selenazole, isoxazole, pyrimidine, quinolone, purine, pyrazolopyrimidine, pyrazoloquinazoline, and some other heterocyclic compounds have been previously synthesized and studied as XO inhibitors [3]. Among them, compounds bearing the carboxyl group like febuxostat appeared to be effective inhibitors of the enzyme. The binding mechanisms of such compounds to the XO active site include the interactions of their carboxylate groups with Arg880 and Thr1011 [3].

The present study is aimed to synthesize the pyrazolone-based 4-(furan-2-yl)benzoic acids for their evaluation as XO inhibitors. It should be noted that structurally similar compounds namely pyrazolone-based phenylfuran-2-yl derivatives were described previously as inhibitors of SARS-CoV and MERS-CoV 3C-like protease [4], heptosyltransferase WaaC [5], and neuraminidase [6].

■ Results and discussion

Compounds **3a**–**i** were synthesized with a yield of 80–87% according to **Scheme** by the Knoevenagel condensation of pyrazolones **1** with 4-(5-formylfuran-2-yl)benzoic acid (**2**). The pyrazolones **1** bearing various substituents in positions 3 and 5 were obtained by the condensation of β-ketocarboxylic esters with hydrazine derivatives (Knorr synthesis) [7]. 4-(5-Formylfuran-2-yl)benzoic acid was obtained *via* the arylation of 2-furancarboxaldehyde by a diazonium salt of *p*-aminobenzoic acid (Meerwein arylation method) [8]. ^{1}H NMR, IR, and mass-spectra confirmed the structures of the compounds **3a**–**i** synthesized. In ^{1}H NMR spectra, the methyne proton (–CH=) signals appear in the range from 8.06 to 6.87 ppm, overlapping with the signals from the aryl substituents (except compound **3g** with the chemical shift of the methine proton singlet of 7.85 ppm). The ^{1}H NMR signals of the carboxylic groups were observed at 12.17–13.11 ppm. In the IR spectra, the intensive absorption bands of carbonyl groups were found at 1679–1696 cm^{-1}.

The synthesized compounds **3a**–**i** can exist as *E*- or *Z*-isomers. It was shown previously that (5-phenylfuran-2-yl)methylene-containing pyrazolone derivatives synthesized by the same route were a mixture of *E*-*Z*-isomers with a *Z*-isomer as a major product [5, 6].

The pyrazolone derivatives **3a**–**i** were studied *in vitro* as inhibitors of xanthine oxidase from bovine milk. This enzyme was characterized by 90% amino acid sequence identity to XO from the human liver [9]. The IC_{50} values determined from the dose-dependent curves of the enzyme inhibition (**Figure 1**) are presented in **Table 1**. These values are inhibitor concentrations, at which the XO activity was decreased by 50%.

According to the results obtained, compounds **3a**–**i** exhibited low micromolar IC_{50} values towards

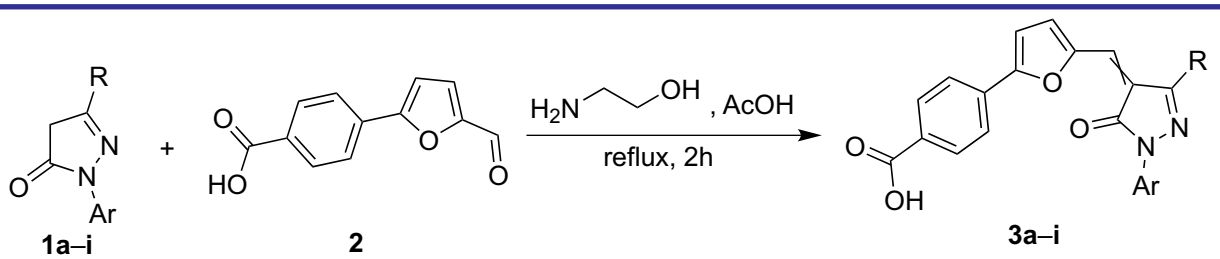

1a, **3a**: Ar = Ph, R = Me
1b, **3b**: Ar = Ph, R = CF_3
1c, **3c**: Ar = Ph, R = Ph
1d, **3d**: Ar = Ph, R = 4-FC_6H_4
1e, **3e**: Ar = Ph, R = 4-ClC_6H_4
1f, **3f**: Ar = Ph, R = 4-$O_2NC_6H_4$
1g, **3g**: Ar = Ph, R = thiophen-2-yl
1h, **3h**: Ar = Ph, R = pyridin-4-yl
1i, **3i**: Ar = 4-MeC_6H_4, R = Ph

Scheme. The synthesis of pyrazolone-based 4-(furan-2-yl)benzoic acids **3a**–**i**

ISSN 2308-8303 (Print) / 2518-1548 (Online)

Table 1. Pyrazolone-based 4-(furan-2-yl)benzoic acids as xanthine oxidase inhibitors*

Compound	IC_{50}, μM	IC_{50}, μM (in the presence of BSA)	IC_{50}, μM (in the presence of Tween-80)
3a	0.036 ± 0.0025	0.09 ± 0.02	0.11 ± 0.01
3b	0.52 ± 0.09	2.54 ± 0.69	2.44 ± 0.37
3c	0.096 ± 0.006	2.16 ± 0.48	3.74 ± 0.43
3d	0.15 ± 0.03	2.32 ± 0.10	2.55 ± 0.12
3e	0.17 ± 0.04	3.30 ± 0.68	7.48 ± 1.04
3f	0.22 ± 0.015	3.77 ± 0.09	7.88 ± 1.42
3g	0.058 ± 0.012	4.66 ± 0.91	2.58 ± 0.25
3h	0.22 ± 0.02	1.87 ± 0.51	2.20 ± 0.29
3i	0.06 ± 0.014	0.63 ± 0.18	2.08 ± 0.33
Febuxostat	0.0062 ± 0.0007	0.0075 ± 0.0001	0.0056 ± 0.0005

Note: *IC_{50} values were determined from 2-3 series of experiments and shown as an average value ± standard deviation. The concentrations of BSA or Tween-80 in the model systems were 2 μM and 0.025 vol. %, respectively

XO *in vitro*. Compound **3a** bearing 3-methyl-5-phenyl pyrazolone part had an IC_{50} value of 36 nM; it was the closest to that for the inhibition by febuxostat (**Table 1**) and significantly exceeded the IC_{50} value (4.5 μM) of 4-(5-formylfuran-2-yl) benzoic acid (**2**) observed. This indicates that the inhibition efficiency of compound **3a** was ensured due to a pyrazolone scaffold. The replacement of the methyl group in the structure of compound **3a** on the trifluoromethyl substituent (derivative **3b**) led to a 14-fold loss of the XO inhibition activity. Compounds **3c**–**h** with phenyl, 4-fluorophenyl, 4-chlorophenyl, 4-nitrophenyl, thiophen-2-yl, or pyridin-4-yl substituents in position 3 of the pyrazolone ring, as well as compound **3i** bearing the 1-(4-tolyl)-3-phenyl-substituted pyrazolone moiety were characterized by low differences in the IC_{50} values ranging from 0.058 to 0.22 μM.

The inhibition effects of most of the compounds studied here were found to be significantly reduced (up to 80-fold) by bovine serum albumin (BSA) or Tween-80 (**Table 1**). The inhibitory activity in the presence of BSA and a detergent was less changed for compound **3a** bearing a methyl group at position 3 of the pyrazolone ring and decreased most strongly for 3-(thiophen-2-yl)-substituted compound **3g**. In contrast to this, BSA or Tween-80 almost did not change the inhibitory potency of febuxostat as a reference compound against XO.

Taking into account that the decrease of the XO inhibition can be related to the binding of the inhibitors to BSA, a spectral study was performed. It was found that compound **3i** quenched the fluorescence of BSA (**Figure 2**).

The BSA fluorescence spectra were measured at different temperatures (298 K, 303 K, 308 K, and 313 K) in the presence of 0.5 μM, 1 μM, 2 μM, and 3 μM of compound **3i**. The Stern-Volmer

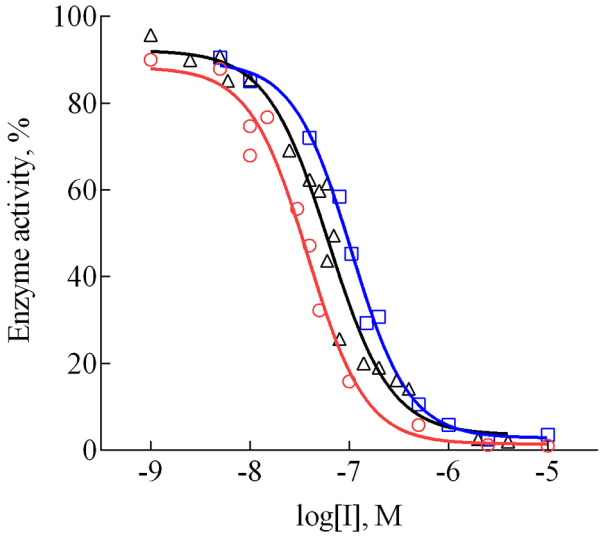

Figure 1. Dose-dependent curves of xanthine oxidase inhibition by compounds **3a** (○), **3c** (□) and **3i** (Δ)

quenching constants (K_{SV}) obtained from plots of F_0/F *vs.* the quencher concentration were 2.55×10^5 M^{-1} ($R^2 = 0.98$), 3.42×10^5 M^{-1} ($R^2 = 0.96$), 5.36×10^5 M^{-1} ($R^2 = 1.00$), 6.42×10^5 M^{-1} ($R^2 = 0.99$), respectively. The K_{SV} values increased with an increase in temperature. This dependence can indicate a dynamic quenching process. However, further analysis showed that the apparent bimolecular quenching rate constants (k_q) were three orders of magnitude larger than the value of the maximum scatter collision quenching constant of various quenchers with biopolymers (2.0×10^{10} M^{-1} sec^{-1}) [10]. The calculated values of k_q were 4.39×10^{13} M^{-1} sec^{-1}, 5.90×10^{13} M^{-1} sec^{-1}, 9.25×10^{13} M^{-1} sec^{-1}, and 1.11×10^{14} M^{-1} sec^{-1} for 298 K, 303 K, 308 K, and 313 K, respectively. Thus, the fluorescence quenching of BSA by compound **3i** can be also caused by the complex formation.

The results of kinetic studies were analyzed to elucidate the mechanism of the XO inhibition

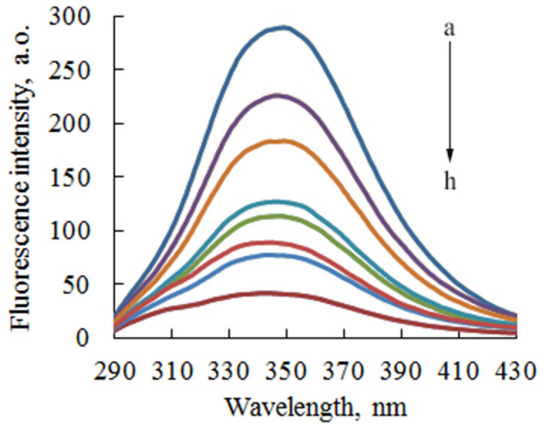

Figure 2. Fluorescence emission spectra of BSA in the absence (**a**) and presence (**b** → **h**) of compound **3i** measured at a temperature of 298 K, λ_{ex} of 280 nm, and slits of 5 nm. The BSA concentration was 2 μM. The concentrations of compound **3i** were 0 μM, 1 μM, 2 μM, 4 μM, 5 μM, 6 μM, 8 μM, and 10 μM

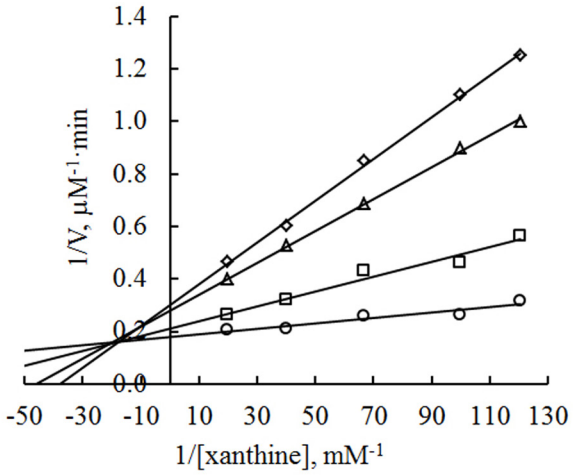

Figure 3. Lineweaver-Burke plots for the XO inhibition by compound **3a**. The inhibitor concentrations were 0 (○), 15 nM (□), 30 nM (Δ), and 45 nM (◊)

by pyrazolone derivative **3a**. The double reciprocal Lineweaver-Burk plots shown in **Figure 3** demonstrate that compound **3a** is a mixed-type inhibitor of the enzyme. The competitive and non-competitive inhibition constants (K_i and K_i') calculated were 7.11 ± 1.27 nM and 66.5 ± 15.4 nM, respectively. The K_i value being one order of magnitude lower than the K_i' value indicates that the affinity of the compound is higher to the free enzyme than to the enzyme-substrate complex.

Molecular docking calculations were carried out using the AutoDock Vina software [11]. The affinity of compound **3a** (*Z*-isomer) to XO was characterized by a docking energy of -10.8 kcal mol^{-1}. According to the results obtained, the 4-(furan-2-yl)benzoic acid fragment of compound **3a** is located in the substrate binding region near the molybdopterin cofactor. The carboxylic group of the inhibitor has a salt-bridge interaction with Arg880, as well as hydrogen bonds with Thr1010 and a water molecule (HOH1457), which interacts with Glu1261. The phenyl group of the 4-(furan-2-yl)benzoic acid part of the inhibitor forms face-to-face and edge-to-face π-π-stacking interactions with Phe914 and Phe1009. The furan linker that connects the benzoic acid and pyrazolone fragments of the inhibitor is sandwiched between hydrophobic amino acid residues Leu873, Leu1014, and Pro1076. The pyrazolone fragment bearing phenyl and methyl groups in position 1 and 3, respectively, is located near Leu648, Phe649, Lys771, His875, Ser876, Val1011, and Phe1013. The oxygen atom of the pyrazolone carbonyl group forms a hydrogen bond with Ser876 (**Figure 4 (A)**).

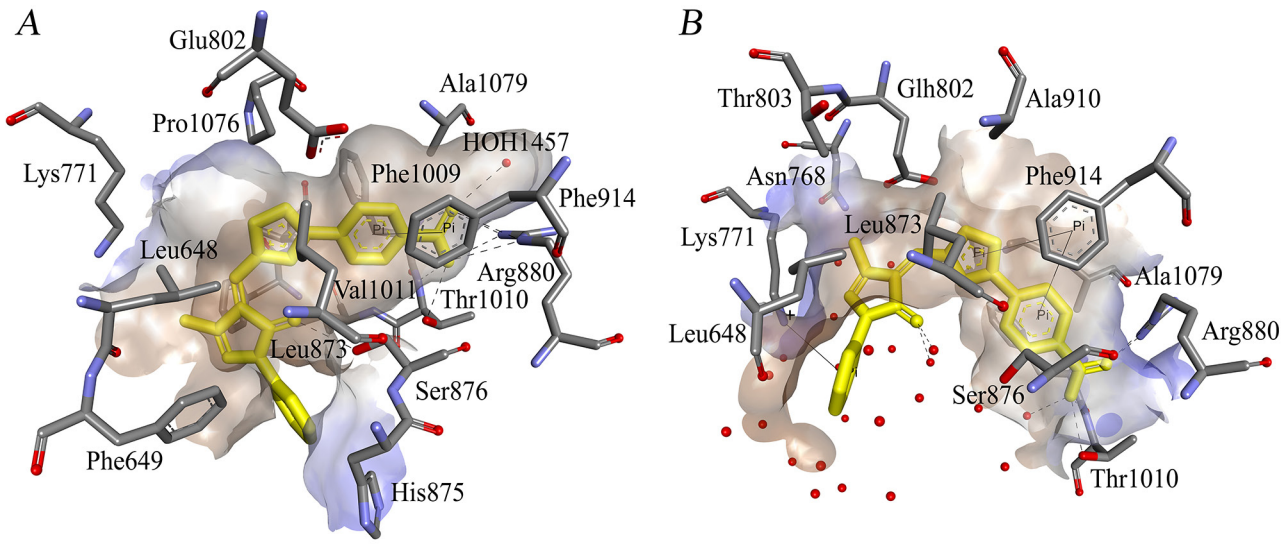

Figure 4. Binding modes of the *Z*-isomer of compound **3a** in the active site of XO predicted by the molecular docking calculation (*A*) and the subsequent molecular dynamic simulation (*B*). All the hydrogens are hidden for clarity, and the oxygen atoms shown as red spheres represent water molecules

ISSN 2308-8303 (Print) / 2518-1548 (Online)

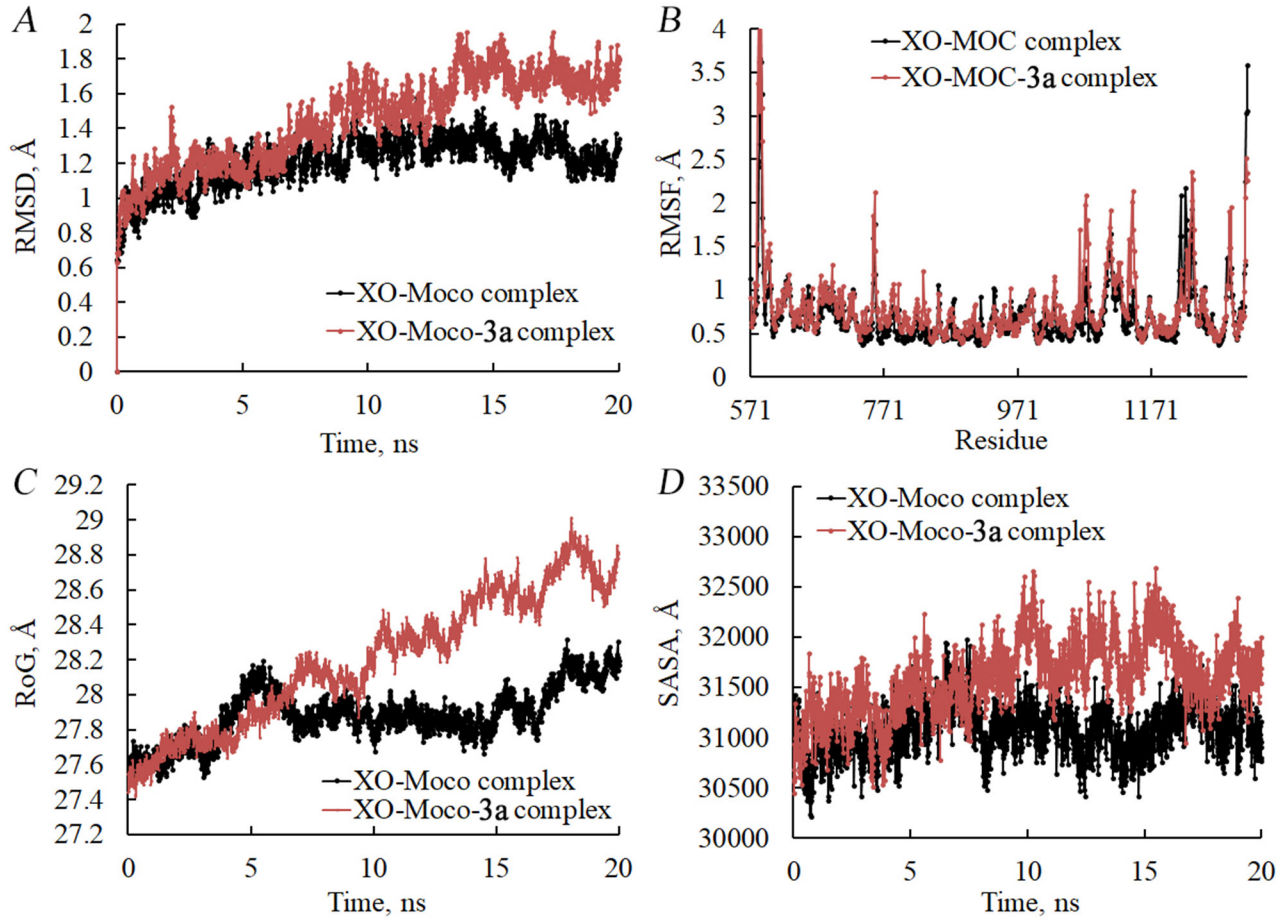

Figure 5. The values of the root mean square deviation of the enzyme backbone (*A*), the root mean square fluctuation of the amino acid residues (*B*), the radius of gyration (*C*), and the solvent accessible surface area (*D*) obtained from the MD simulation for the XO-Moco and XO-Moco-**3a** model systems

The molecular dynamic simulation was performed by the NAMD software [12] to verify the stability of the enzyme-inhibitor complex model obtained, as well as for a more detailed analysis of the interactions that could occur between inhibitor **3a** and the enzyme active site. The calculations were performed with the complex of the chain C of the enzyme containing molybdopterin and the inhibitor (XO-Moco-**3a**), as well as with the complex of the chain C of XO containing only a molybdopterin cofactor (XO-Moco). The time-dependent changes of the root mean square deviation (RMSD) values for the enzyme backbone atoms for both model systems are shown in **Figure 5 (A)**. As can be seen, the RMSD of XO-Moco and XO-Moco-**3a** complexes reached equilibration approximately after 10 ns and 14 ns, respectively. The XO-Moco-**3a** model system has higher RMSD values compared to those for the XO-Moco complex. This suggests that the binding of the ligand leads to a change in the structure of the enzyme. Despite this, the root mean square fluctuation (RMSF) revealed that compound **3a** only slightly affected the fluctuation of the nearby amino acid residues (**Figure 5 (B)**). The negative effect of the ligand on the compactness and folding of XO is indicated by the increased values of the radius of gyration (RoG) and solvent-accessible surface area (SASA) which are shown in **Figure 5 (C)** and **Figure 5 (D)**, respectively.

The binding mode of inhibitor **3a** in the active site of the XO obtained after 20 ns of the MD simulation is given in **Figure 4 (B)**. The ligand is more deeply located in the active site of the enzyme as compared with its location after the molecular docking (**Figure 4 (A)**). This is especially noticeable from the changed locations of the furan ring and the 3-methyl-5-phenyl substituted pyrazolone moiety, which showed π-π-stacking and π-cation interactions with Phe914 and Lys771, respectively. Such position of the inhibitor can be caused by the solvent action of water forming hydrogen bonds with the carbonyl oxygen of the pyrazolone ring. The changes in the structure of the enzyme detected by the plots in **Figure 5** can be related to the changes in the position of the inhibitor. According to several studies [13, 14, 15] and the check of the amino acid residues protonation states by the PROPKA software [16], Glu802 was protonated, and therefore, was represented as Glu802.

The free binding energy of compound **3a** in the active site of the XO was studied from the MD simulation results using the MMPBSA method. As seen from **Table 2**, the VDWAALS, EEL, and ENPOLAR energies contribute to stabilization of the enzyme-inhibitor complex, while the EPB and EDISPER energies lead to its destabilization.

The free energy decomposed by the MMPBSA method per amino acid residues located within 4 Å from the ligand in the enzyme active site at the last frame of the MD simulation are shown in **Table 3**. Currently, the method cannot be used for the decomposition of the non-polar solvation component. According to the total energies, the interactions of the benzoic acid moiety of the ligand with the amino acid residues Arg880, Phe1009, and Thr1010 are key factor for the enzyme-inhibitor complex stabilization. As can be seen, the electrostatic energies make the greatest contribution to these interactions.

Table 2. The calculated energies of MMPBSA components of the free binding energy of compound **3a** bound at the XO active site*

MMPBSA component	Energy ± SD, kcal mol^{-1}
VDWAALS	-34.5398 ± 3.1316
EEL	-101.2729 ± 14.6772
EPB	106.1432 ± 10.5794
ENPOLAR	-28.9013 ± 1.6140
EDISPER	49.3169 ± 1.9125
ΔG_{total}	-11.3089 ± 6.7691

Note: *VDWAALS is a van der Waals energy contribution from MM; EEL is the electrostatic energy as calculated by the MM force field; EPB is an electrostatic contribution to the solvation free energy calculated by PB; ENPOLAR is a nonpolar contribution to the solvation free energy calculated by an empirical model; EDISPER is dispersion energy; ΔG_{total} is the free binding energy.

Conclusions

Thus, pyrazolone-based 4-(furan-2-yl)benzoic acids **3a**–**i** can inhibit XO with IC_{50} values in the submicromolar range. The inhibitory properties of the compounds are affected by the nature of substituents in position 3 of the pyrazolone ring. The inhibition of XO by most of the compounds synthesized is significantly reduced in the presence of bovine serum albumin or Tween-80, excluding 3-methyl-1-phenyl pyrazolone-based derivative **3a**. Among the 4-(furan-2-yl)benzoic acids synthesized, compound **3a** has proven to be a potent inhibitor of xanthine oxidase. Kinetic studies have shown that the 3-methyl-1-phenyl pyrazolone-based 4-(furan-2-yl)benzoic acid **3a** is a mixed-type inhibitor of the enzyme. The inhibition constants calculated suggest that the affinity of the inhibitor to the free enzyme is higher than that to the enzyme-substrate complex. Molecular docking and molecular dynamic simulations have shown that the salt-bridge and the hydrogen bond formed between the carboxylic group of the inhibitor and the residues Arg880 and Thr1010 can be responsible for the stability of the enzyme-inhibitor complex.

Experimental part

Commercially available chemical reagents and solvents were purchased and used without purification. The TCL method was applied to monitor the reaction progress. The Fisher-Johns apparatus was used for the melting point determination. ^{1}H NMR spectra were taken on a Varian Mercury (500 MHz) spectrometer in DMSO-d_6 or $CF_3C(O)OD$ solution using the signal of residual

Table 3. The free energy decomposed per amino acid residues

Residue	Energy ± SD, kcal mol^{-1}			
	van der Waals	Electrostatic	Polar solvation	TOTAL
Leu648	-1.64 ± 0.57	-0.03 ± 0.30	0.65 ± 0.48	-1.02 ± 0.44
Asn768	-0.37 ± 0.15	-0.16 ± 0.27	0.88 ± 0.43	0.35 ± 0.44
Lys771	-1.05 ± 0.41	-15.21 ± 2.196	17.21 ± 2.97	0.94 ± 0.92
Glh802	-0.90 ± 0.33	-0.51 ± 0.24	1.78 ± 0.47	0.37 ± 0.46
Thr803	-0.21 ± 0.12	-0.18 ± 0.08	0.24 ± 0.11	-0.15 ± 0.11
Leu873	-1.83 ± 0.30	0.85 ± 0.17	-0.59 ± 0.16	-1.57 ± 0.33
Ser876	-1.37 ± 0.20	-0.12 ± 1.16	1.97 ± 1.10	0.47 ± 0.49
Arg880	0.13 ± 0.78	-39.28 ± 5.73	32.42 ± 2.62	-6.74 ± 3.77
Ala910	-0.18 ± 0.10	-0.57 ± 0.08	0.56 ± 0.11	-0.19 ± 0.15
Phe914	-1.30 ± 0.34	0.11 ± 0.24	0.23 ± 0.29	-0.96 ± 0.28
Phe1009	-2.03 ± 0.37	-5.35 ± 0.87	4.27 ± 0.35	-3.12 ± 0.94
Thr1010	0.43 ± 0.83	-12.82 ± 3.65	6.80 ± 1.68	-5.59 ± 1.92
Ala1078	-0.87 ± 0.24	-0.80 ± 0.37	1.00 ± 0.28	-0.68 ± 0.35
Ala1079	-1.09 ± 0.33	-0.38 ± 0.58	1.13 ± 0.49	-0.34 ± 0.46

ISSN 2308-8303 (Print) / 2518-1548 (Online)

solvent protons as a standard. IR spectra were recorded on a Vertex-70 spectrometer in KBr tablets. LC-MS spectra were obtained using an Agilent 1200 Series high-performance liquid chromatograph.

4-(5-Formyl-2-furanyl)benzoic acid **2** was obtained by the method described previously [17].

The general procedure for the synthesis of compounds 3a–i

A solution of 0.005 mol of corresponding pyrazolone **1** in 15–20 mL of acetic acid was added to a hot solution of 0.005 mol of 4-(5-formyl-2-furanyl)benzoic acid **2** in 20–30 mL of acetic acid followed by addition of 0.005 mol of ethanolamine. The reaction mixture was refluxed for 2 hours and then left at 20–25 °C for 12 hours. The precipitate formed was filtered, washed with ethanol, dried, and recrystallized from a mixture of MeCN/DMF.

4-[5-(3-Methyl-5-oxo-1-phenyl-1,5-dihydropyrazol-4-ylidenemethyl)-furan-2-yl]-benzoic acid (**3a**)

E/*Z* – 1:3. Burgundy solid. Yield – 86%. M. p. > 250 °C. Anal. Calcd for $C_{22}H_{16}N_2O_4$, %: C 70.96, H 4.33, N 7.52. Found, %: C 70.90, H 4.38, N 7.44. IR (KBr), ν_{max}, cm^{-1}: 2873, 1680 (C=O), 1604, 1319, 1273, 1027. ^1H NMR (500 MHz, DMSO-d_6), δ, ppm: 2.31 (0.75H, s, Me), 2.68 (0.25H, s, Me), 7.18 (1H, t, J_{HH} = 8.0 Hz, Ar), 7.49–7.66 (2H, m, Ar), 7.75–8.00 (4H, m, Ar, –CH=), 8.00–8.05 (4H, m, Ar), 8.64 (1H, d, J_{HH} = 4.0 Hz, Ar), 13.03 (1H, br. s, C(O)OH). LC-MS, *m*/*z* (I_{rel}, %): 373 $[M+H]^+$ (100).

4-[5-(5-Oxo-1-phenyl-3-trifluoromethyl-1,5-dihydro-pyrazol-4-ylidenemethyl)-furan-2-yl]-benzoic acid (**3b**)

Z-isomer. Burgundy solid. Yield – 82%. M. p. > 250 °C. Anal. Calcd for $C_{22}H_{13}F_3N_2O_4$, %: C 61.98, H 3.07, N 6.57. Found, %: C 62.04, H 3.16, N 6.50. IR (KBr), ν_{max}, cm^{-1}: 2535, 1692 (C=O), 1590, 1510, 1470, 1427, 1276, 1116, 954, 808. ^1H NMR (500 MHz, DMSO-d_6), δ, ppm: 7.33 (1H, t, J_{HH} = 8.0 Hz, Ar), 7.50–7.53 (2H, m, Ar, –CH=), 7.68–7.72 (1H, m, Ar), 7.82–7.87 (3H, m, Ar), 8.07–8.17 (4H, m, Ar), 8.80–8.82 (1H, m, Ar), 13.09 (1H, br. s, C(O)OH). LC-MS, *m*/*z* (I_{rel}, %): 427 $[M+H]^+$ (100).

4-[5-(5-Oxo-1,3-diphenyl-1,5-dihydro-pyrazol-4-ylidenemethyl)-furan-2-yl]-benzoic acid (**3c**)

E/*Z* – 1:5. Burgundy solid. Yield – 85%. M. p. > 250 °C. Anal. Calcd for $C_{27}H_{18}N_2O_4$, %: C 74.65, H 4.18, N 6.45. Found, %: C 74.74, H 4.22, N 6.40. IR (KBr), ν_{max}, cm^{-1}: 2545, 1696 (C=O), 1591, 1275, 942, 802. ^1H NMR (500 MHz, DMSO-d_6), δ, ppm: 7.00 (1H, d, J_{HH} = 8.0 Hz, Ar), 7.25 (1H, t, J_{HH} = 8.0 Hz, Ar), 7.48 (2H, q, J_{HH} = 8.0 Hz, Ar), 7.61–7.79 (6H, m, Ar, –CH=), 7.78 (2H, d, J_{HH} = 8.0 Hz, Ar), 8.76–7.96 (5H, m, Ar), 12.17 (1H, br. s, C(O)OH). LC-MS, *m*/*z* (I_{rel}, %): 436 $[M+H]^+$ (100).

4-{5-[3-(4-Fluoro-phenyl)-5-oxo-1-phenyl-1,5-dihydro-pyrazol-4-ylidenemethyl]-furan-2-yl}-benzoic acid (**3d**)

E/*Z* – 1:5. Burgundy solid. Yield – 85%. M. p. > 250 °C. Anal. Calcd for $C_{27}H_{17}FN_2O_4$, %: C 71.68, H 3.79, N 6.19. Found, %: C 71.72, H 3.82, N 6.12. IR (KBr), ν_{max}, cm^{-1}: 2989, 1696 (C=O), 1591, 1496, 1275, 944, 810. ^1H NMR (500 MHz, DMSO-d_6), δ, ppm: 7.01 (1H, d, J_{HH} = 8.0 Hz, Ar), 7.22–7.32 (2H, m, Ar), 7.43–7.51 (4H, m, Ar), 7.64–7.86 (4H, m, Ar, –CH=), 7.95–8.76 (5H, m, Ar), 12.12 (1H, br. s, C(O)OH). LC-MS, *m*/*z* (I_{rel}, %): 453 $[M+H]^+$ (100).

4-{5-[3-(4-Chloro-phenyl)-5-oxo-1-phenyl-1,5-dihydro-pyrazol-4-ylidenemethyl]-furan-2-yl}-benzoic acid (**3e**)

E/*Z* – 1:3. Burgundy solid. Yield – 80%. M. p. > 250 °C. Anal. Calcd for $C_{27}H_{17}ClN_2O_4$, %: C 69.16, H 3.65, Cl 7.56, N 5.97. Found, %: C 69.34, H 3.72, Cl 7.60, N 5.94. IR (KBr), ν_{max}, cm^{-1}: 2536, 1683 (C=O), 1592, 1274, 941, 803, 771. ^1H NMR (500 MHz, DMSO-d_6), δ, ppm: 6.96–7.27 (1H, m, Ar), 7.46–7.52 (3H, m, Ar), 7.61–7.86 (6H, m, Ar, –CH=), 7.94–8.08 (5H, m, Ar), 8.75 (1H, d, J_{HH} = 4.0 Hz, Ar), 13.08 (1H, br. s, C(O)OH). LC-MS, *m*/*z* (I_{rel}, %): 470 $[M+H]^+$ (100).

4-{5-[3-(4-Nitro-phenyl)-5-oxo-1-phenyl-1,5-dihydro-pyrazol-4-ylidenemethyl]-furan-2-yl}-benzoic acid (**3f**)

E/*Z* – 1:5. Burgundy solid. Yield – 80%. M. p. > 250 °C. Anal. Calcd for $C_{27}H_{17}N_3O_6$, %: C 67.64, H 3.57, N 8.76. Found, %: C 67.68, H 3.64, N 8.72. IR (KBr), ν_{max}, cm^{-1}: 2535, 1687 (C=O), 1592, 1516, 1348, 1273, 803. ^1H NMR (500 MHz, DMSO-d_6), δ, ppm: 6.87-8.06 (6H, m, Ar, –CH=), 8.22–8.41 (2H, m, Ar), 8.74 (8H, m, Ar), 13.05 (br. s, 1H, C(O)OH). LC-MS, *m*/*z* (I_{rel}, %): 480 $[M+H]^+$ (100).

4-[5-(5-Oxo-1-phenyl-3-thiophen-2-yl-1,5-dihydro-pyrazol-4-ylidenemethyl)-furan-2-yl]-benzoic acid (**3g**)

Z-izomer. Burgundy solid. Yield – 80%. M. p. > 250 °C. Anal. Calcd for $C_{25}H_{16}N_2O_4S$, %: C 68.17, H 3.66, N 6.36, S 7.28. Found, %: C 68.24, H 3.76, N 6.46, S 7.32. IR (KBr), ν_{max}, cm^{-1}: 2531, 1682 (C=O), 1593, 1422, 1277, 693. ^1H NMR (500 MHz, DMSO-d_6), δ, ppm: 7.22 (2H, t, J_{HH} = 8.0 Hz, Ar), 7.30 (1H, t, J_{HH} = 4.0 Hz, Ar), 7.45 (2H, t, J_{HH} = 8.0 Hz, Ar), 7.58 (1H, d, J_{HH} = 4.0 Hz, Ar), 7.76–7.85 (3H, m, Ar, –CH=), 7.91–8.03 (5H, m, Ar), 8.72 (1H, d, J_{HH} = 4.0 Hz, Ar), 13.40 (1H, br. s, C(O)OH). LC-MS, *m*/*z* (I_{rel}, %): 441 $[M+1]^+$ (100).

4-[5-(5-Oxo-1-phenyl-3-pyridin-4-yl-1,5-dihydro-pyrazol-4-ylidenemethyl)-furan-2-yl]-benzoic acid (**3h**)

E/*Z* – 1:5. Burgundy solid. Yield – 85%. M. p. > 250 °C. Anal. Calcd for $C_{26}H_{17}N_3O_4$, %: C 71.72, H 3.94, N 9.65. Found, %: C 71.86, H 4.00, N 9.60. IR (KBr), ν_{max}, cm^{-1}: 2920, 2567, 1670 (C=O), 1602, 1510, 1400, 1265, 931, 807. ^1H NMR (500 MHz, $CF_3C(O)OD$), δ, ppm: 7.42–7.80 (7H, m, Ar, –CH=), 8.21–8.75 (7H, m, Ar), 9.22–9.30 (2H, m, Ar). LC-MS, *m*/*z* (I_{rel}, %): 436 $[M+H]^+$ (100).

4-[5-(5-Oxo-3-phenyl-1-p-tolyl-1,5-dihydro-pyrazol-4-ylidenemethyl)-furan-2-yl]-benzoic acid (**3i**)

E/*Z* – 1:5. Burgundy solid. Yield – 87%. M. p. > 250 °C. Anal. Calcd for $C_{28}H_{20}N_2O_4$, %: C 74.99, H 4.50, N 6.25. Found, %: C 74.90, H 4.67, N 6.30. IR (KBr), ν_{max}, cm^{-1}: 2923, 2536, 1679 (C=O), 1603, 1513, 1424, 1276, 943, 812. ^1H NMR (500 MHz, DMSO-d_6), δ, ppm: 2.33 (3H, s, Me), 7.29 (2H, d, J_{HH} = 8.0 Hz, Ar), 7.60–7.64 (5H, m, Ar, –CH=), 7.78 (2H, d, J_{HH} = 8.0 Hz, Ar), 7.88 (2H, t, J_{HH} = 8.0 Hz, Ar), 8.05–8.77 (5H, m, Ar), 13.11 (1H, br. s, C(O)OH). LC-MS, *m*/*z* (I_{rel}, %): 449 $[M+H]^+$ (100).

The *in vitro* study of pyrazolone-containing 4-(furan-2-yl)benzoic acids as xanthine oxidase inhibitors

XO from bovine milk and xanthine as a substrate were purchased from Sigma-Aldrich. In the case of pyrazolone-based 4-(furan-2-yl)benzoic acids **3a**–**i**, the system contained a sodium-phosphate buffer (50 mM, pH 7.4), xanthine (50 μM), EDTA (0.1 mM), DMSO (1%), and an inhibitor. To study the specificity of the XO inhibition by compounds **3a**–**i**, the reaction mixture additionally contained 2 μM of BSA or 0.025 vol. % Tween-80. The reaction was initiated by the enzyme addition after preincubation of the mixture for 5 min. The total volume of the system was 2 mL. The activity of XO was monitored spectrophotometrically at 293 nm. The uric acid molar extinction coefficient of 12.2 mM^{-1} cm^{-1} was used for calculations. The value of the calculated Michaelis-Menten constant (K_m) was 5.7 μM.

The fluorescence quenching experiment

The fluorescence quenching studies were performed on the example of compound **3i** to confirm the interaction of pyrazolone-based 4-(furan-2-yl) benzoic acids with bovine serum albumin (BSA). The reaction mixture consisted of sodium phosphate buffer (50 mM, pH 7.4), 2 μM BSA, DMSO (1%), and a quencher (compound **3i**). The total volume of the reaction mixture was 2 mL. The Stern-Volmer quenching constants were obtained from plots of F_0/F *vs.* the quencher concentration described by the Stern-Volmer equation:

$$F_0 / F = 1 + k_q\tau_0 = 1 + K_{SV}[Q]$$

where F_0 and F are the BSA fluorescence intensities observed without and with the quencher in the model systems, respectively; [*Q*] is the concentration of the quencher; k_q is the apparent bimolecular quenching rate constant; τ_0 is the lifetime of unquenched tryptophan in BSA; K_{SV} is the Stern-Volmer quenching constant.

Molecular docking calculation

Compound **3a** was docked into the active site (chain C) of XO from bovine milk (PDB code 1FIQ [9]) using the protocol described in [18]. The calculation was performed by the AutoDock Vina software [11]. The enzyme-inhibitor model complex was analyzed by Discovery Studio 3.5 (Accelrys, San Diego, CA, USA).

Molecular dynamic simulation

The molecular dynamic simulations were performed using the NAMD software [12] according to the previously described protocol [19]. The preparation of the model system for the calculation was carried out using the conda environment. The VMD 1.9.3 [20] was used for the calculation of RMSD, RMSF, RoG, and SASA. The binding free energy and its decomposition per amino acid residues were performed by MMPBSA.py [21] according to the protocol described in [19].

Acknowledgements

We would like to thank Enamine Ltd for supporting the synthesis of compounds.

References

1. Chen, C.; Lü, J.-M.; Yao, Q. Hyperuricemia-related diseases and xanthine oxidoreductase (XOR) inhibitors: an overview. *Med. Sci. Monit.* **2016**, *22*, 2501–2512. https://doi.org/10.12659/msm.899852.
2. Singh, A.; Singh, K.; Sharma, A.; Kaur, K.; Chadha, R.; Bedi, P. M. S. Past, present and future of xanthine oxidase inhibitors: design strategies, structural and pharmacological insights, patents and clinical trials. *RSC Med. Chem.* **2023**, *14*, 2155–2191. https://doi.org/10.1039/D3MD00316G.
3. Šmelcerović, A.; Tomović, K.; Šmelcerović, Ž.; Petronijević, Ž.; Kocić, G.; Tomašič, T.; Jakopin, Ž.; Anderluh, M. Xanthine oxidase inhibitors beyond allopurinol and febuxostat; an overview and selection of potential leads based on in silico calculated physico-chemical properties, predicted pharmacokinetics and toxicity. *Eur. J. Med. Chem.* **2017**, *135*, 491–516. https://doi.org/10.1016/j.ejmech.2017.04.031.
4. Kumar, V.; Tan, K.-P.; Wang, Y.-M.; Lin, S.-W.; Liang, P.-H. Identification, synthesis and evaluation of SARS-CoV and MERS-CoV 3C-like protease inhibitors. *Bioorg. Med. Chem.* **2016**, *24* (13), 3035–3042. https://doi.org/10.1016/j.bmc.2016.05.013.

ISSN 2308-8303 (Print) / 2518-1548 (Online)

5. Moreau, F.; Desroy, N.; Genevard, J. M.; Vongsouthi, V.; Gerusz, V.; Le Fralliec, G.; Oliveira, C.; Floquet, S.; Denis, A.; Escaich, S.; Wolf, K.; Busemann, M.; Aschenbrenner, A. Discovery of new Gram-negative antivirulence drugs: structure and properties of novel *E. coli* WaaC inhibitors. *Bioorg. Med. Chem. Lett*. **2008**, *18* (14), 4022–4026. https://doi.org/10.1016/j.bmcl.2008.05.117.
6. Kumar, V.; Chang, C.-K.; Tan, K.-P.; Jung, Y.-S.; Chen, S.-H.; Cheng, Y.-S. E.; Liang, P.-H. Identification, synthesis, and evaluation of new neuraminidase inhibitors. *Org. Lett*. **2014**, *16* (19), 5060–5063. https://doi.org/10.1021/ol502410x.
7. Knorr L. Knorr pyrazole synthesis. *Justus Liebigs Ann. Chem*. **1887**, *238*, 137.
8. Racanè, L.; Tralić-Kulenović, V.; Boykin, D.; Karminski-Zamola, G. Synthesis of new cyano-substituted bis-benzothiazolyl arylfurans and arylthiophenes. *Molecules* **2003***, 8* (3), 342–349. https://doi.org/10.3390/80300342.
9. Enroth, C.; Eger, B. T.; Okamoto, K.; Nishino, T.; Nishino, T.; Pai, E. F. Crystal structures of bovine milk xanthine dehydrogenase and xanthine oxidase: structure-based mechanism of conversion. *Proc. Natl. Acad. Sci. USA* **2000**, *97*, 10723–10728. https://doi.org/10.1073/pnas.97.20.10723.
10. Maurice, R. E.; Camillo, A. G. Fluorescence quenching studies with proteins. *Anal. Biochem*. **1981**, *114* (2), 199 – 227. https://doi.org/10.1016/0003-2697(81)90474-7.
11. Trott, O.; Olson, A. J. AutoDock Vina: improving the speed and accuracy of docking with a new scoring function, efficient optimization, and multithreading. *J. Comput. Chem.* **2010**, *31* (2), 455–461. https://doi.org/10.1002/jcc.21334.
12. Phillips, J. C.; Hardy, D. J.; Maia, J. D. C.; Stone, J. E.; Ribeiro, J. V.; Bernardi, R. C.; Buch, R.; Fiorin, G.; Henin, J.; Jiang, W.; McGreevy, R.; Melo, M. C. R.; Radak, B. K.; Skeel, R. D.; Singharoy, A.; Wang, Y.; Roux, B.; Aksimentiev, A.; Luthey-Schulten, Z.; Kale, L. V.; Schulten, K.; Chipot, C.; Tajkhorshid, E. Scalable molecular dynamics on CPU and GPU architectures with NAMD. *J. Chem. Phys*. **2020**, *153* (4), 044130. https://doi.org/10.1063/5.0014475.
13. Okamoto, K.; Eger, B.T.; Nishino, T.; Kondo, S.; Pai, E. F.; Nishino, T. An extremely potent inhibitor of xanthine oxidoreductase. *J. Biol. Chem.* **2002**, *278* (3), 1848–1855. https://doi.org/10.1074/jbc.M208307200.
14. Metz, S.; Thiel, W. A combined QM/MM study on the reductive half-reaction of xanthine oxidase: substrate orientation and mechanism. *J. Am. Chem. Soc.* **2009**, *131* (41), 14885–14902. https://doi.org/10.1021/ja9045394.
15. Ribeiro, P. M.; Fernandes, H. S.; Maia, L. B.; Sousa, S.; Moura, J. J. G. J.; Cerqueira, N. M. F. S. A. The complete catalytic mechanism of xanthine oxidase: a computational study. *Inorg. Chem. Front.* **2021**, *8* (2), 405–416. https://doi.org/10.1039/D0QI01029D.
16. Li, H.; Robertson, A. D.; Jensen, J. H. Very fast empirical prediction and rationalization of protein pKa values. *Proteins* **2005**, *61* (4), 704–721. https://doi.org/10.1002/prot.20660.
17. Varshney, M.; Husain, A.; Parcha, V. Synthesis and characterization of 5-(substituted phenyl)-2-furfuraldehydes from substituted anilines. *World J. Pharmacy Pharm. Sci.* **2013**, *2*(4), 1802–1806.
18. Kobzar, O. L.; Tatarchuk, A. V.; Mrug, G. P.; Bondarenko, S. P.; Demydchuk, B. A.; Frasinyuk, M. S.; Vovk, A. I. Carboxylated chalcones and related flavonoids as inhibitors of xanthine oxidase. *Med. Chem. Res.* **2023**, *32* (8), 1804–1815. https://doi.org/10.1007/s00044-023-03109-8.
19. Beiko, A.V.; Kobzar, O. L.; Kachaeva, M. V.; Pilyo, S. G.; Kozachenko, O. P.; Vovk, A. I. Rhodanine-based 4-(furan-2-yl)benzoic acids as inhibitors of xanthine oxidase. *Ukr. Bioorg. Acta* **2023**, *18* (2), 39–46.
20. Humphrey, W.; Dalke, A.; Schulten, K. VMD – visual molecular dynamics. *J. Mol. Graphics* **1996**, *14*, 33–38. https://doi.org/10.1016/0263-7855(96)00018-5.
21. Miller, B. R.; McGee, T. D.; Swails, J. M.; Homeyer, N.; Gohlke, H.; Roitberg, A. E. MMPBSA.py: an efficient program for end-state free energy calculations. *J. Chem. Theory Comput*. **2012**, *8* (9), 3314–3321. https://doi.org/10.1021/ct300418h.

Information about the authors:

Alona V. Beiko, Ph.D. Student, V. P. Kukhar Institute of Bioorganic Chemistry and Petrochemistry of the NAS of Ukraine; https://orcid.org/0000-0003-1119-988X.

Oleksandr L. Kobzar, Ph.D. in Chemistry; Senior Researcher of the Department of Bioorganic Mechanisms, V. P. Kukhar Institute of Bioorganic Chemistry and Petrochemistry of the NAS of Ukraine; https://orcid.org/0000-0003-4370-7041.

Maryna V. Kachaeva, Ph.D. in Chemistry; Researcher of the Department of Chemistry of Bioactive Nitrogen-Containing Heterocyclic Bases, V. P. Kukhar Institute of Bioorganic Chemistry and Petrochemistry of the NAS of Ukraine; https://orcid.org/0000-0003-1517-4807.

Stepan G. Pilyo, Ph.D. in Chemistry; Senior Researcher of the Department of Chemistry of Bioactive Nitrogen-Containing Heterocyclic Bases, V. P. Kukhar Institute of Bioorganic Chemistry and Petrochemistry of the NAS of Ukraine; https://orcid.org/0000-0002-7089-1393.

Vsevolod Yu. Tanchuk, Ph.D. in Chemistry; Senior Researcher of the Department of Bioorganic Mechanisms, V. P. Kukhar Institute of Bioorganic Chemistry and Petrochemistry of the NAS of Ukraine; https://orcid.org/0000-0001-9055-870X.

Andriy I. Vovk (*corresponding author*), Dr. Sci. in Chemistry, Professor, Head of the Department of Bioorganic Mechanisms, Director of V. P. Kukhar Institute of Bioorganic Chemistry and Petrochemistry of the NAS of Ukraine; https://orcid.org/0000-0001-6167-076X; e-mail for correspondence: vovk@bpci.kiev.ua.